PHYSICAL REVIEW B **73**, 014513 (2006)

Electron doping in MgB_2 studied by electron energy-loss spectroscopy

R. F. Klie,* J. C. Zheng, and Y. Zhu
Center for Functional Nanomaterials, Brookhaven National Laboratory, Upton, New York 11973, USA

A. J. Zambano and L. D. Cooley
Department of Materials Science, Brookhaven National Laboratory, Upton, New York 11973, USA
(Received 29 September 2005; published 17 January 2006)

The electronic structure of electron-doped polycrystalline $Mg_{1-x}Al_x(B_{1-y}C_y)_2$ was examined by electron energy-loss spectroscopy (EELS) in a scanning transmission electron microscope (STEM) and first-principle electronic structure calculations. We found significant changes in the boron *K* edge fine structure, suggesting the two bands of the B *K* edge, the σ and the π band, are being simultaneously filled as the electron doping concentration of $Mg_{1-x}Al_x(B_{1-y}C_y)_2$ was increased. Our density-functional theory calculations confirm the filling of the σ band states close to the Fermi level, which is believed to cause the loss of superconductivity in highly doped MgB_2, since the electron-phonon coupling of these states is thought to be responsible for the high superconducting transition temperature. Our results do not show significant differences in the electronic structure for electron doping on either the Mg or the B site, although many superconducting properties, such as T_c or H_{c_2} differ considerably for C- and Al-doped MgB_2. This behavior cannot be satisfactorily explained by band filling alone, and effects such as interband scattering are considered.

DOI: 10.1103/PhysRevB.73.014513 PACS number(s): 74.70.Ad, 68.37.Lp, 79.20.Uv, 74.25.Jb

INTRODUCTION

Since its discovery as a conventional BCS superconductor with an unexpectedly high superconducting transition temperature (T_c) of 39 K,[1] MgB_2 has been studied intensely over the last 4 years, and many of its properties are now well understood. As such, it was established very early that MgB_2 has four separate sheets at the Fermi surface, two of them being degenerate and corresponding to a two-dimensional σ band and two comprising three-dimensional π bands.[2,3] The different electron-phonon coupling strengths of these bands lead to two distinct superconducting gaps, with the σ band gap having the higher electron-phonon coupling and thus being the main contributor to the unusually high T_c. It was further shown that T_c could be decreased significantly by replacing Mg with Al or B with C,[4–14] which was explained by many different mechanisms ranging from band filling,[15,16] to a merging of the superconducting gaps,[17] to increased interband scattering and a decrease in the electron-phonon coupling strength.[18] While many different mechanisms are now being discussed in the literature, there has not yet been any consistent explanation for the loss of T_c for Al- or C-doped MgB_2. It was previously shown that adding electrons to MgB_2, by doping with Al or C, reduces the bond length (i.e., the unit-cell volume decreases as a function of doping concentration), which lowers the density of states (DOS) and simultaneously stiffens the available phonon modes.[18] However, the effect of decreased lattice parameters, as evidenced by measurements of T_c versus pressure, does not by itself explain the full T_c decrease measured for Al- or C-doped MgB_2.[19] Alternative mechanisms for the decrease of T_c, such as increased interband scattering due to the doping atoms or band filling, have been proposed but no experimental evidence has been reported. Indeed, initial band structure calculations for Al- and C-doped MgB_2 suggested that the decrease in T_c can be understood by simple band filling, caused by the extra electrons provided to the system.[15] Although the effects of Al and C doping on T_c and the superconducting gaps seem to be remarkably similar, other superconducting properties, such as the upper critical field (H_{c_2}), show completely different behavior. In particular, it was shown that H_{c_2} is dramatically increased in both poly-crystalline $Mg(B_{1-y}C_y)_2$ and especially in thin-film samples.[20] On the other hand, $Mg_{1-x}Al_xB_2$ shows only a weak increase in H_{c_2} for small concentrations of Al, and otherwise a significant decrease.[21]

Kortus *et al.*[15] pointed out that the experimental data on both doped and "pure" MgB_2 show a large spread of properties, e.g., T_c of 10% C-doped MgB_2 ranges between 12 K and 34 K depending on the synthesis and annealing conditions. Moreover, the exact doping concentration of the MgB_2 grains is not measured directly in most studies, but rather measurements that average over many grains are performed. Therefore, a systematic study of the effects of C and Al doping on the electronic structure and the superconducting properties, with doping concentrations measured inside the $Mg_{1-x}Al_x(B_{1-y}C_y)_2$ grains, is needed to fully understand its complex structure-property relationships. Also, most conventional electronic-structure measurements, such as x-ray absorption spectroscopy (XAS), cannot study individual grains or distinguish between different crystallographic orientations, since no **large** single crystals of Al- or C-doped MgB_2 have been available to date. Thus, we need to use electronic structure probes that are significantly smaller than the grain size of $Mg_{1-x}Al_x(B_{1-y}C_y)_2$ in order to accurately measure the effects of doping on the local DOS and its anisotropy.

In this paper, we explore the electronic structure of Al- and C-doped MgB_2 by combined high-resolution *Z*-contrast imaging and electron energy-loss spectroscopy (EELS) in a scanning transmission electron microscope (STEM). Our

previous work[22–24] showed how these two techniques can be used to study the electronic structure of individual grains of MgB_2; here we apply them to quantify the changes as a function of either Al or C doping. In particular, orientation-resolved EELS will allow us to distinguish the behavior of the π and σ band for the different doping concentrations. The samples of $Mg_{1-x}Al_xB_2$ and $Mg(B_{1-y}C_y)_2$ were previously characterized for their superconducting properties;[10,25] we will correlate the changes in the measured electronic structure with these properties. Moreover, we use first-principles calculations to compare the changes in the EELS spectra to those in the density of unoccupied B p states for the different doping concentrations and explore the filling of the σ band close to the Fermi level.

EXPERIMENTAL SETUP

The results presented in this paper were obtained using a JEOL3000F transmission electron microscope (TEM), equipped with an ultra-high-resolution (UHR) objective lens pole piece, a Fischione high-angle annular dark-field (HAADF) detector, a post column Gatan imaging filter (GIF), and a NORAN x-ray detector. The instrument is capable of being operated in either the conventional TEM or scanning TEM (STEM) mode. For the atomic resolution imaging and analysis results shown here, the incoherent HAADF imaging mode (or Z-contrast imaging) in the STEM was used exclusively. The key to atomic resolution in STEM microscopy[26–29] is the formation of the smallest possible electron probe with sufficient probe current (40 pA) to obtain statistically significant images and spectra. The electron probe is optimized using the electron "Ronchigram," or "shadow image" (for a more detailed description see Refs. 26 and 30), to obtain a probe-size of $\sim$1.5 Å for these experiments.

The experimental setup of this microscope allows the low-angle scattered electrons to be used, which do not contribute to the Z-contrast image, for electron energy-loss spectroscopy (EELS).[31] As the two techniques do not interfere, this means that Z-contrast images can be used to position the electron probe at the desired spot on the sample while acquiring spectra.[26,32,33] The lens conditions in the microscope and spectrometer were set up for the smallest probe size, with a convergence angle (α) of 11 mrad, a detector inner angle of 30 mrad, and an EELS spectrometer collection angle (θ_c) of 25 mrad.

The physical principle behind EELS relates the interaction of fast electrons with the sample to cause either collective excitations of electrons in the conduction bands (plasmons) or discrete transitions between atomic energy levels.[31] In this study we will focus on the the latter class, using boron (B) K edge core-loss spectra, which is comprised of transitions from the B 1s states into the unoccupied B 2p states above the Fermi energy (E_F). In the experiment performed here, EEL spectra of the B K edge are acquired directly from grains in the [110] and [001] orientations with an acquisition time of 3 s per spectrum. The experimental spectra shown here are a sum of 15 individual spectra, added to increase the signal-to-noise ratio of the near-edge fine structure. Further, unless stated otherwise, the background is subtracted from each spectrum and the resulting data are then deconvoluted with the zero-loss peak to remove the effects of plural scattering from the core-loss spectra.[31]

TABLE I. Transition temperature (T_c), sintering temperature (T_s), sintering time (t_s), and lattice parameters (a,c) for the different samples.

Sample	T_c (K)	T_s (°C)	t_s (h)	a (Å)	c (Å)
MgB_2	35.0	1200	96	3.082	3.521
$Mg(B_{0.96}C_{0.04})_2$	32.0	1200	48	3.069	3.520
$Mg(B_{0.92}C_{0.08})_2$	24.5	950	1	3.047	3.519
$Mg_{0.85}Al_{0.15}B_2$	29.3	1200	96	3.077	3.476
$Mg_{0.75}Al_{0.25}B_2$	7.2	1200	96	3.066	3.424

The simulated EELS spectra shown in this paper are calculated using first-principles methods based on density functional theory (DFT).[34,35] We used the newly updated `TELNES.2` package included in the `WIEN2K` code,[36] a full-potential linear augmented plane-wave (FLAPW) plus local-orbitals method within DFT. The generalized gradient approximation (GGA) proposed by Perdew, Burke, and Ernzerhof[37] was used for the exchange correlation. Muffin-tin radii (r_{MT}) were 2.00 bohr for Mg, and 1.65 bohr for B, and $r_{MT}k_{max}$ was taken to be 7.0. The angular momentum (l) expansion up to l_{max} for the potential and charge density representations was used in the calculations. At convergence, the integrated difference between input and output charge densities was less than 10^{-4}. For all structures, 252 k points in the irreducible Brillouin zone were used in the calculations. We used the experimental lattice parameters, as given in Table I, in our calculations of the EELS fine structure for the different doping concentrations.

SAMPLE PREPARATION

The $Mg_{1-x}Al_x(B_{1-y}C_y)_2$ samples for this study were prepared using various reaction and sintering conditions to create material with a homogeneous distribution of the doping element, minimize secondary phases such as MgB_4, MgO, AlB_x, or MgC_x, and maximize the grain size. Here, we will only briefly describe the different sintering conditions for the various samples, while more detailed descriptions can be found elsewhere.[10,25,38] Undoped MgB_2 and $Mg_{1-x}Al_xB_2$ samples were prepared in a high-temperature process that lasted for nearly 96 h, with thorough annealing to obtain homogeneity. Initially, the appropriate mixture of Mg, B, and Al powders was heated to 1200 °C and kept at this temperature for 1 h. The temperature was then decreased to 700 °C at a rate of 0.1 °C min^{-1} and kept at 700 °C for 5 h. Finally, the sample was brought to room temperature at a rate of 20 °C min^{-1}.[10] The resulting materials have an average grain-size of >1 μm and do not show show a significant number of impurity or secondary phases.

The $Mg(B_{0.96}C_{0.04})_2$ sample was prepared from a carbon-doped B fiber by Ames Laboratory.[38] The $Mg(B_{0.92}C_{0.08})_2$ sample was made by mixing the appropriate ratio of Mg and

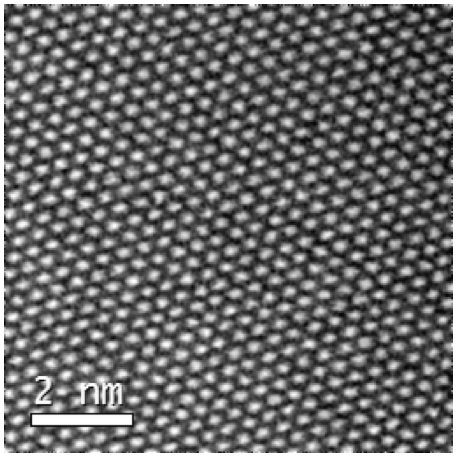

FIG. 1. High-resolution Z contrast of 25% Al-doped MgB_2 [001] with no apparent superstructure due to Al ordering.

B_4C powders and subsequently heating it to 950 °C for 1 h followed by slow cooling. X-ray diffraction analysis of this material showed the presence of a small concentration of Mg_2C_3 impurity phases.

For all the samples studied here, we found that the doping concentration within the grains that were studied appears to be homogeneous, and no ordering of the dopants was found in any sample. We found that the precise doping concentration varies slightly from grain to grain, in particular, in those samples with shorter sintering time. We used EDX and EELS analyses to determine the doping concentration of the individual grains probed, and the respective doping concentration given for each sample in this paper applies only to the individual grains that were studied. Figure 1 shows an example of a typical high-resolution Z-contrast image of a grain in the [001] projection found in $Mg_{0.75}Al_{0.25}B_2$. Similar images can be obtained for all other doping concentrations. The bright spots in this image show the Mg/Al columns in this projection of the MgB_2 structure. Due to the small scattering amplitude at large scattering angles, the B columns are not visible in this image. Since the image intensity is proportional to $Z^{1.7}$, and Al ($Z=13$) is slightly heavier than Mg ($Z=12$), while C ($Z=6$) is slightly heavier than B ($Z=5$), ordering or clustering of the Al or C atoms would be visible in such Z-contrast images as variations of the atomic column contrast. For instance, oxygen ordering in grains of MgB_2 on the B sublattice was previously observed by similar Z-contrast imaging.[23] This makes it likely that ordering or clustering of dopants should also be visible here. From Fig. 1, which is shown here as a representation of all other doping concentrations, it can be clearly seen that no superstructure due to dopant ordering can be found. A summary of the properties of the different sample materials used in this study is given in Table I.

RESULTS

Figures 2(a) and 2(b) show the B K edge core-loss EELS spectra for the different Al-doping concentrations. The spectra are aligned at the edge onset for undoped MgB_2, which is

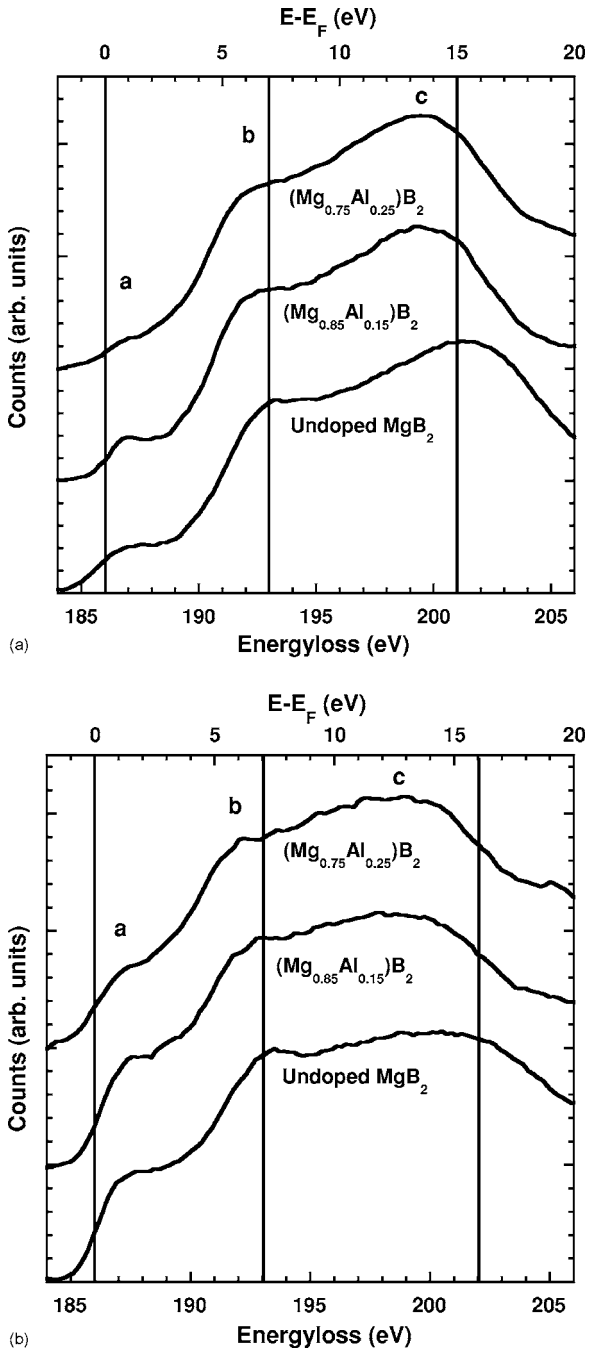

FIG. 2. EELS of B K edge for different Al-doping concentrations from grains in the (a) [001] and (b) [110] orientation.

located at 186.0 eV, and are further offset in the vertical direction to clearly show the differences in the near-edge fine structure for the different doping concentrations. In this projection the experimental B K edge spectrum contains three major features or peaks within the first 20 eV above the edge onset. The small shoulder or pre-peak intensity is labeled throughout this paper as peak a; the pre-peak is followed by a shoulder of higher intensity at ~193 eV in pristine MgB_2 and is labeled peak b. The main feature of the B K edge, which is located at 202 eV, represents a broad peak without any further fine structure and is labeled peak c. We have added three vertical lines to all the figures containing EELS

spectra, at the edge onset (186 eV), the position of peak *b* (193 eV), and the broader peak *c* at 202 eV in pristine MgB_2. Figure 2(a) shows the spectra taken from $Mg_{1-x}Al_xB_2$ grains in the [001] projection.

With increasing Al concentration, it can be clearly seen from Fig. 2(a) that peaks *b* and *c* are shifting towards lower energies. In addition, the peak intensities change for the different doping concentrations: the pre-edge peak intensity (*a*) decreases significantly for $Mg_{0.85}Al_{0.15}B_2$ and is nearly completely vanished for $Mg_{0.75}Al_{0.25}B_2$. Further, the intensity of peak *c* seems to be increased for both $Mg_{0.85}Al_{0.15}B_2$ and $Mg_{0.75}Al_{0.25}B_2$.

The spectra from grains in the [110] orientation [Fig. 2(b)] are very different from those of the [001] orientation. The most obvious difference is the higher pre-peak intensity (peak *a*) in the [110] orientation compared to the [001] orientation, and we have previously discussed these differences in the context of the two bands of the boron *p* states in MgB_2.[22,39] However, the spectra in the [110] orientation show similar trends as seen in the [001] orientation, in particular the energy shifts of peaks *b* and *c* as well as the decrease in the intensity of the pre-edge peak *a*. While this pre-edge peak intensity decreases as a function of Al doping, it is still clearly visible for $Mg_{0.75}Al_{0.25}B_2$. In undoped MgB_2, peak *b* is clearly visible, while for $Mg_{0.75}Al_{0.25}B_2$ it is barely noticeable as a shoulder at ~191.8 eV.

Figures 3(a) and 3(b) show the calculated EELS spectra for $Mg_{1-x}Al_xB_2$ in the [001] and [110] orientation using the virtual crystal approximation (VCA). Unlike previously published spectra, these calculations take into consideration the experimental unit-cell volume which might be considerably different from the calculated ones, and this results in significant changes of the near-edge fine structure of the calculated spectra. The theoretical spectra shown here are smoothed by a Gaussian function with 0.8 eV width at half-maximum to simulate the instrument resolution. The simulated EELS spectrum for undoped MgB_2 shows good agreement with the experimental results, in that the positions of peaks *a* and *b* are reproduced accurately, as well as decrease in intensity of peak *a* for increasing Al concentration. For the [001] orientation [Fig. 3(a)], the energy position of peak *c* is slightly higher in the calculated spectra, and the energy shift of peaks *b* and *c* appears to be slightly smaller than in the experimental spectra. Figure 3(b) shows more structure of the pre-peak *a* than seen in the experimental spectra, and peak *b* is not distinguishable from the broader shoulder that appears at 198.5 eV in the calculated spectrum of pristine MgB_2. This peak is not visible in the experimental spectra, and the intensity of peak *c* at 201.5 eV is underestimated by the theoretical spectra. However, the peak at 198.5 eV becomes stronger and more distinct with increasing Al concentration, while no changes can be seen for the peak at 201.5 eV.

The B *K* edge EELS spectra for C-doped MgB_2 are shown in Figs. 4(a) and 4(b), where undoped MgB_2 is compared to $Mg(B_{0.96}C_{0.04})_2$ and $Mg(B_{0.92}C_{0.08})_2$ in the two crystal orientations, [001] and [110]. Similar to the Al-doped samples, the B *K* edge in C-doped MgB_2 shows a measurable decrease in the peak intensity of the pre-peak *a* in both crystal orientations, and a small shift of peak *b* in the spectra from $Mg(B_{1-y}C_y)_2$ grains as the C concentration is increased.

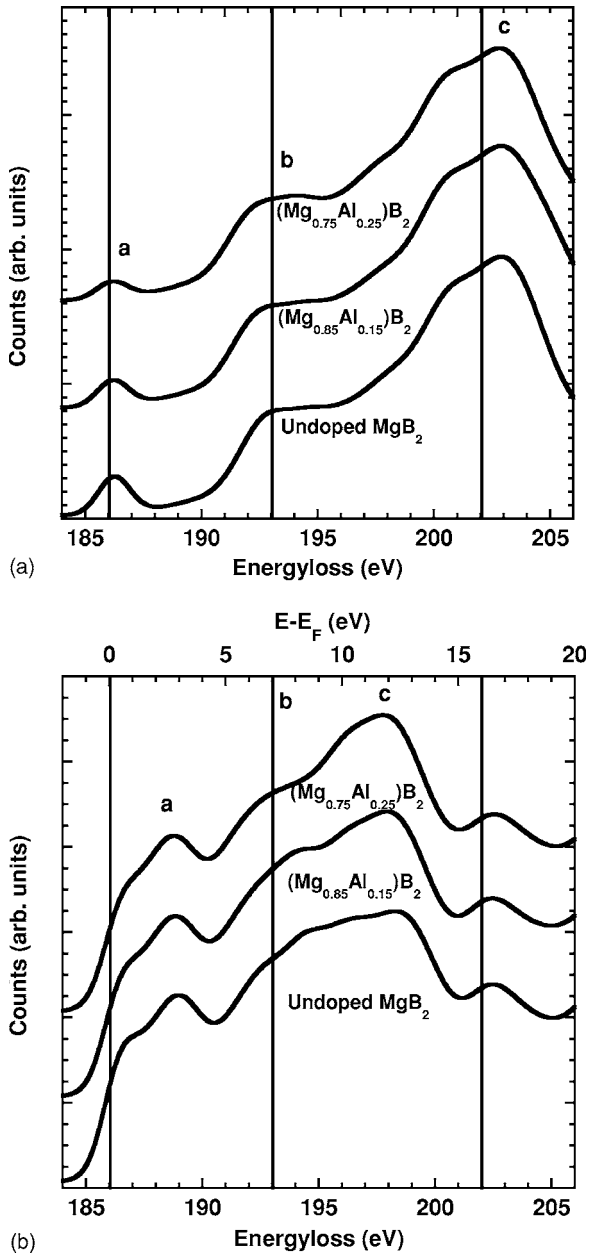

FIG. 3. Calculated B *K* edge for different Al-doping concentrations using DFT with VCA for grains in the (a) [001] and (b) [110] orientation.

While peak *c* shifts downwards in energy for $Mg(B_{0.92}C_{0.08})_2$ there is no noticeable shift of peak *c* in $Mg(B_{0.96}C_{0.04})_2$. However, with increasing C-doping concentration one can observe an increase in the intensity of peak *c*, which is located at 202 eV in pristine MgB_2. The spectra from grains in the [110] orientation [Fig. 4(b)] show a shift in energy of peak *b*, but no measurable shift of peak *c* as a function of C doping. In addition to this shift, peak *b* (at 193.5 eV in MgB_2) becomes more distinguishable for higher C concentrations; a similar trend can be seen for the broader peak *c*.

The results of the DFT calculations for C-doped MgB_2 in the [001] and [110] orientation, shown in Figs. 5(a) and 5(b), are in general agreement with the experimental spectra. In the calculation of these spectra, the VCA was used and the

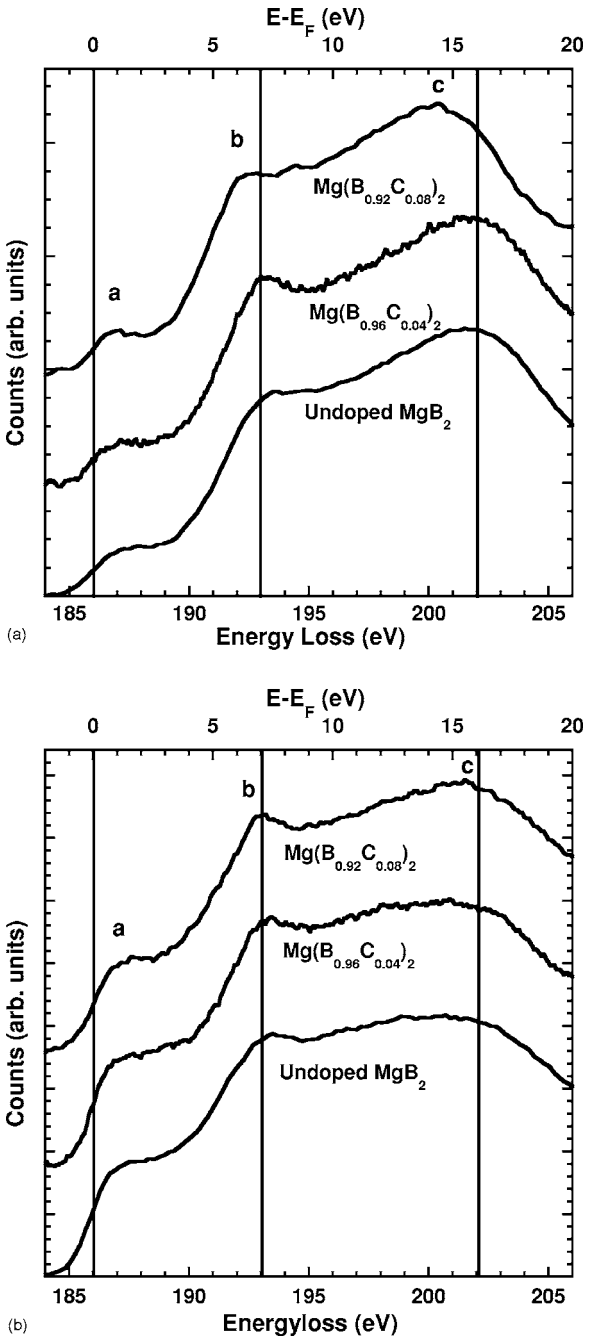

FIG. 4. EELS of B *K* edge for different C-doping concentrations from grains in the (a) [001] and (b) [110] orientation

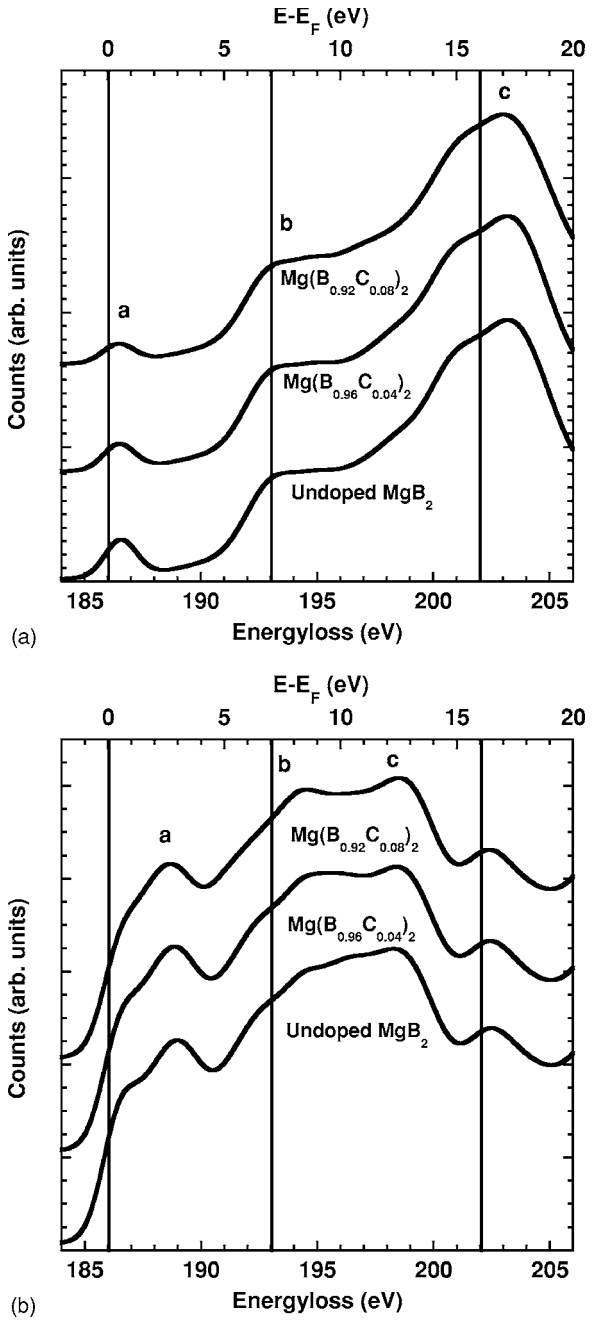

FIG. 5. Calculated B *K* edge for different C-doping concentrations using DFT with VCA for grains in the (a) [001] and (b) [110] orientation.

resulting spectra were broadened by 0.8 eV to match the experimental energy resolution. Figure 5(a) shows the decrease in the pre-peak intensity (peak *a*) with increasing C concentration and a small shift of peak *c* towards lower energy for $Mg(B_{0.92}C_{0.08})_2$. However, the calculated spectra show an intensity of peak *b* that is significantly lower than measured experimentally. The calculations for the [110] orientations [Fig. 5(b)] show a decrease in the pre-peak intensity and reflect the positions of peak *b* adequately. However, neither the position of peak *c* nor the shape and intensity of peak *b* are reproduced in the calculated spectra. Similar to Fig. 3(b), the calculated spectra show an additional intensity at 198.5 eV, while underestimating the intensity of peak *c*. Further, the peak at 198.5 eV increases in intensity as the C-doping concentration is increased.

While many of the general changes in the first 15–20 eV of the B *K* edge fine structure are well reproduced by the DFT calculations, the intensity of peak *b* at ~193 eV and peak *c* in the [110] orientation are only poorly reflected in the theoretical spectra. We have previously shown that the peak at 193 eV is correlated to oxygen-rich areas in MgB_2 or even amorphous BO_x principates or surfaces layers.[23,24,40] Since we could not observe any superlattice structure in the MgB_2 grains that would indicate O inside the MgB_2 grain, it

is reasonable to assume that the exposure of the samples to air has caused the formation of an amorphous boron-oxide layer at the top and bottom surfaces. The shift of this peak at ~193.0 eV is an artifact of the postacquisition energy-scale alignment, and further indicates a shift in the Fermi level upon doping MgB_2 with electron.

DISCUSSION

In order to interpret the changes in the B *K* edge fine structure as a function of Al and C doping, a complete understanding of the orientation dependance of the B *K* edge is needed. It has been shown previously that the B *K* edge near-edge fine structure of MgB_2 will change significantly as a function of grain orientation with respect to the incoming electron probe [as shown in Figs. 2(a) and 2(b) or Figs. 4(a) and 4(b)] due to the fact that MgB_2 is an anisotropic material.[22,24,39] Since MgB_2 is a layered compound with graphite-like layers of B atoms and intercalated Mg layers, the orientation of the electron probe with respect to these layers can excite different transitions as the angle between the electron probe and the two-dimensional B layer changes. We have previously shown that two crystal orientations, [001] and [110] (i.e., perpendicular and parallel to the hexagonal B layers), are sufficient to separate the contributions of the boron σ and the π bands.[22,39] For EELS core-loss spectra that have been acquired from MgB_2 grains in the [001] projection, we have shown the majority of the spectral contribution (~90%) stems from the transitions perpendicular to the incoming beam direction, i.e., promoting the B 1*s* electron into the unoccupied σ band. For grains in the [110] orientation, only half the observed intensity comes from those σ band transitions, the other half is made up by transitions into the π band. This can be understood by considering the fact that we use a highly convergent electron probe and a large spectrometer acceptance angle, which means that there is significant momentum transfer into transition perpendicular to the incoming beam direction.[22]

Figure 6 shows the density of states (DOS) in the vicinity of E_F as computed by DFT for undoped MgB_2. The unoccupied σ states have high intensity at E_F that drops to zero within 0.8 eV above E_F. The DOS of the σ band then remains low up to ~5 eV above E_F and finally increases to form the σ^* peak at 192.0 eV. Meanwhile, the π states have a nearly flat distribution of the DOS as the energy increases from 186 to 193 eV, with the exception of the small peak at 189 eV. As described above, any experimental EELS spectrum will contain contributions from both of those bands,[22,41] which means that the pre-peak in the experimental spectra contains transitions from the B 1*s* states into the sum of the high density of unoccupied σ and the flat π states at E_F, while peak *b* contains transitions into the σ^* at ~192 eV. The changes in the B *K* edge fine structure for the different crystal orientations can be best understood by a varying mixture of the σ and the π states to the total B *K* edge spectrum.

The superconducting properties of MgB_2, in particular T_c, are strongly correlated to the high density of σ states close to the Fermi level, and the the dominance of these transitions in the spectra from the [001] orientation gives us a unique experimental window, through which the electronic structure important for superconductivity can be accessed. It is widely believed that filling of these σ states by electron doping will decrease the density of superconducting carriers (which are holes), and thus T_c should decrease. The filling of the empty *p* states will result in an increase in the Fermi level, and one would expect that $T_c=0$ *K* once all the σ states are filled (i.e., the Fermi level shifted by more than 0.8 eV). This shift in the Fermi level should result in a chemical shift of the B *K* edge as well as a decrease in the pre-edge peak intensity. Indeed, this is exactly what is seen in Figs. 2(a) and 4(a).

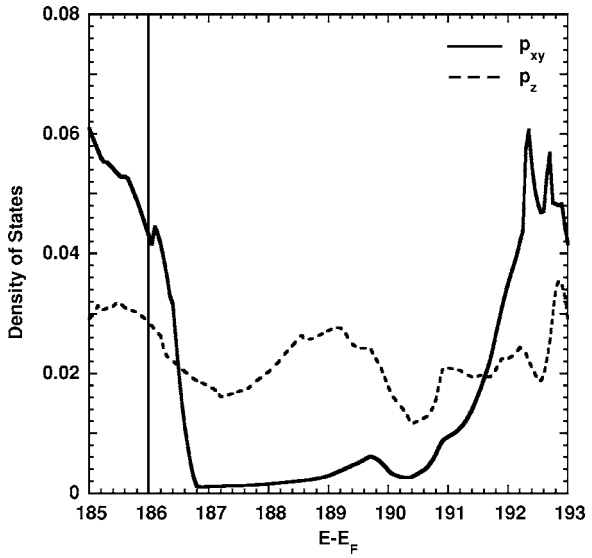

FIG. 6. Density of boron *p* states in the vicinity of the Fermi level. The Fermi energy (E_F) is shown at 186 eV, while the two separate bands are shown between −1.0 and 7.0 eV with respect to the Fermi energy.

To quantify the changes in the B *K* edge, we will use the spectra from the [001] orientation only, since they provide us with the majority of σ state transitions, and either the chemical shift or the pre-peak intensity can be used to correlate the hole-state density to the superconducting properties. However, since the energy resolution of the experimental EELS spectra is only ~1.0 eV and a chemical shift of 0.8 eV is sufficient to fill most of the available σ states, we will use the pre-peak intensity as a more reliable measure. A Gaussian function was used to fit the pre-edge peak at 0–1 eV above E_F; three more Gaussian functions were then used to fit the remaining peaks of the B *K* edge. Figure 7(a) shows the spectrum for undoped MgB_2 and a fit of the experimental data using four Gaussians of varying width and intensity. The pre-peak intensity of the experimental spectrum consists of a Gaussian located at 186 eV, while the σ^* peak is formed by one Gaussian at 192 eV and a broader Gaussian at 195 eV. Similarly, we have fitted all the experimental spectra of the different Al- and C-doping concentrations shown in Figs. 2(a) and 4(a). Figure 7(b) shows the relative pre-peak intensity as calculated from the Gaussian fits for the different Al- and C-doping concentrations. The pre-peak intensity is normalized to the fitted σ^* peak intensity to account for variations in sample thickness or acquisition times. Similarly, we have fitted four Gaussian functions to all the calculated spec-

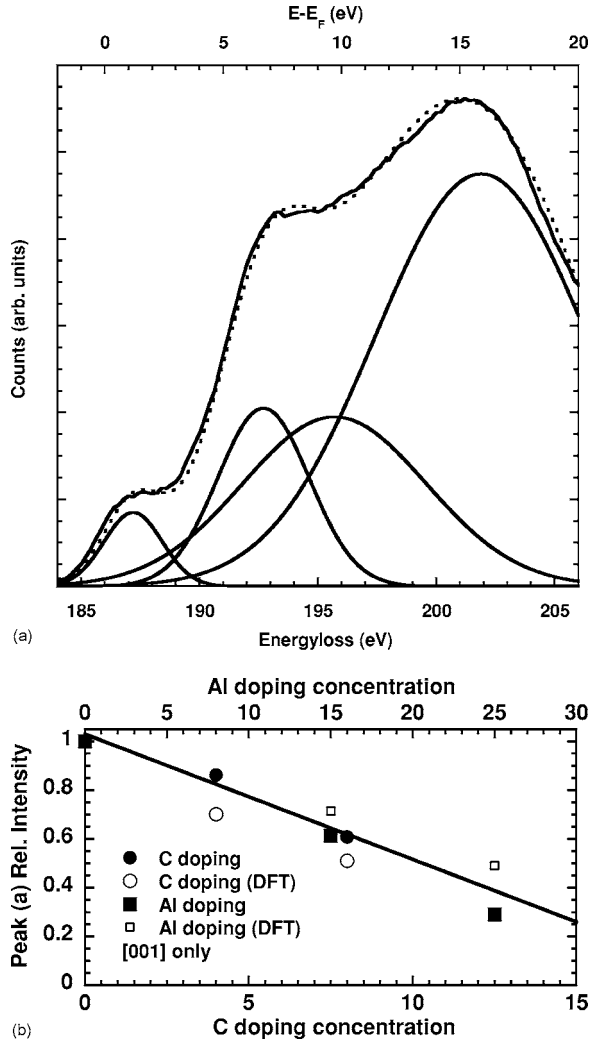

FIG. 7. (a) Example of the four-Gaussian fit (dotted line) with the experimental data (solid line) for undoped MgB_2, used to calculate the decrease in pre-peak intensity relative the σ^* peak as a function of electron doping. (b) Relative pre-peak intensity as a function of electron doping as a result of the four-Gaussian fit. The open symbols represent the theoretical and the full symbols the experimental results; the least-square fit is shown as a solid line.

tra shown in Figs. 3(a) and 5(a). We can clearly see that within the experimental uncertainty the pre-peak intensities for both Al- and C-doped concentrations decrease linearly with increasing doping concentration, and the least square fit is plotted in Fig. 7(b). Thus, for the first time there is direct spectroscopic evidence that band filling occurs as MgB_2 is doped with electrons. Extrapolating the linear fit in Fig. 7(b), one will find that relative pre-peak intensity will vanish completely at $x_{crit}^{EELS} \sim 40\%$ Al doping or $y_{crit}^{EELS} \sim 20\%$ C. This means that all the empty σ states close to E_F will be filled completely at $x > 40\%$ Al doping, thus resulting in a collapse of the high-temperature two-band superconductivity in $Mg_{1-x}Al_xB_2$.[25] It has been previously reported that x_{crit} (the Al composition at which $T_c \rightarrow 0$ *K*) is at $\sim 33\% - 40\%$. However, y_{crit} (the C composition at which $T_c \rightarrow 0$ K) has been measured to be $\sim 12\% - 25\%$.[15] This means that within the experimental uncertainties $x_{crit}^{obs} \approx x_{crit}^{EELS}$, but $y_{crit}^{obs} < y_{crit}^{EELS}$.

This means that, although the changes in the B *K* edge spectra for Al- and C-doped MgB_2 appear to be very similar, there seems to be a fundamental difference in the mechanism that governs the measured loss of superconductivity in doped MgB_2 for these dopants. The drop in T_c with increasing Al concentration can be successfully explained in terms of band filling, while the simple band-filling picture appears to underestimate the decrease in T_c in C-doped MgB_2. Similarly, Kortus *et al.*[15] reported that the larger decrease of T_c in C-doped MgB_2 can be explained by an increased interband scattering rate, while the effect of Al doping on T_c is simply due to band filling. Further, the authors argue that the two superconducting gaps in $Mg(B_{1-y}C_y)_2$ merge, resulting in an additional lowering of T_c of about 6 K in MgB_2 with 10%–15% C doping.

For a more in-depth look at the changes in the electronic structure of electron-doped MgB_2, we have calculated the density of states and the band structure for the compounds we have studied experimentally. Figure 8(a) shows the partial DOS of the σ and the π bands for MgB_2, $Mg_{0.85}Al_{0.15}B_2$, and $Mg_{0.75}Al_{0.25}B_2$; Fig. 8(b) shows the band structure for the same compounds in the vicinity of the Fermi level containing the π, the σ, and the σ^* bands. The DOS of the σ band for Al-doped MgB_2 [Fig. 8(a)] shows a decrease of the high density of states at the Fermi level that is closely related to the measured pre-peak intensity change. Further, the σ^* peak at ~ 6 eV above E_F shifts towards lower energies with increasing Al-doping concentration. The highest peak in this energy range located at 17.5 eV above E_F [and corresponds to peak *c* in Fig. 2(a)] does not exhibit any visible shift, but increases in intensity as the Al concentration is increased. The empty π band states do not show any significant change for the different doping concentrations.

The band structure [Fig. 8(b)] reveals some further details related to the changes in the electronic structure upon Al doping. Here, the high intensity at E_F in the σ band corresponds to the flat band close to the Fermi level between Γ and *A*, while the σ^* peak corresponds to the flat band ~ 6 eV above E_F. It can be clearly seen that with increasing Al concentration the σ band close to E_F shifts lower in energy and at 25% the band at Γ is nearly completely submerged under the Fermi level. The density of states at the Γ point is particularly important, since it is these states at the Brillouin zone (BZ) center that couple to the E_{2g} phonons and create the high T_c. Further, the σ^* band appears to be shifting faster in energy than the bands close to E_F as the Al concentration increases, thus indicating a nonrigid shift of the σ bands applies. On the other hand, there appears to be hardly any shift of the π bands, which are located at *K* in the BZ. Interestingly, this means that the extra electrons provided by the Al substituting for Mg fill only the σ hole-states rather than the π band. Therefore, this filling of the σ states, albeit nonrigid, can account for the decrease in T_c that was previously reported.[15,25]

The DOS for the π and σ states of C-doped MgB_2 are shown in Fig. 9(a). Similarly to DOS of $Mg_{1-x}Al_xB_2$ the high intensity in the σ states close to the Fermi level is decreasing significantly upon C doping. While the hole-states at E_F shift below the Fermi level with increasing C concentration, the σ^* peak at ~ 6 eV above E_F does not seem to shift at all.

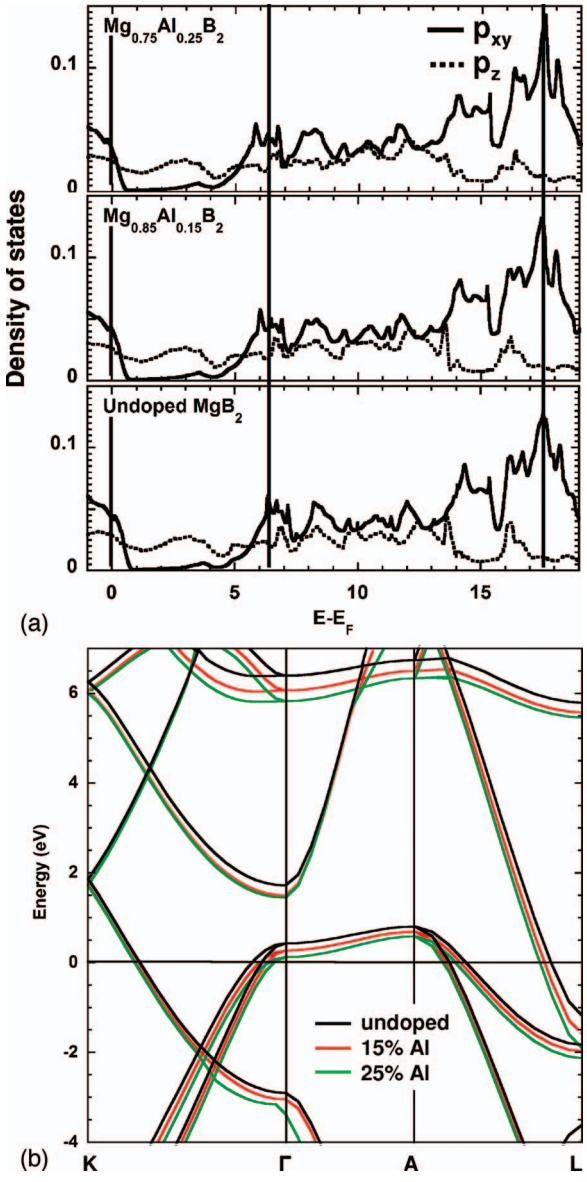

FIG. 8. (Color) Calculated (a) partial density of states and (b) band structure of pristine and Al-doped MgB_2 showing the σ-band shift for the different doping concentrations.

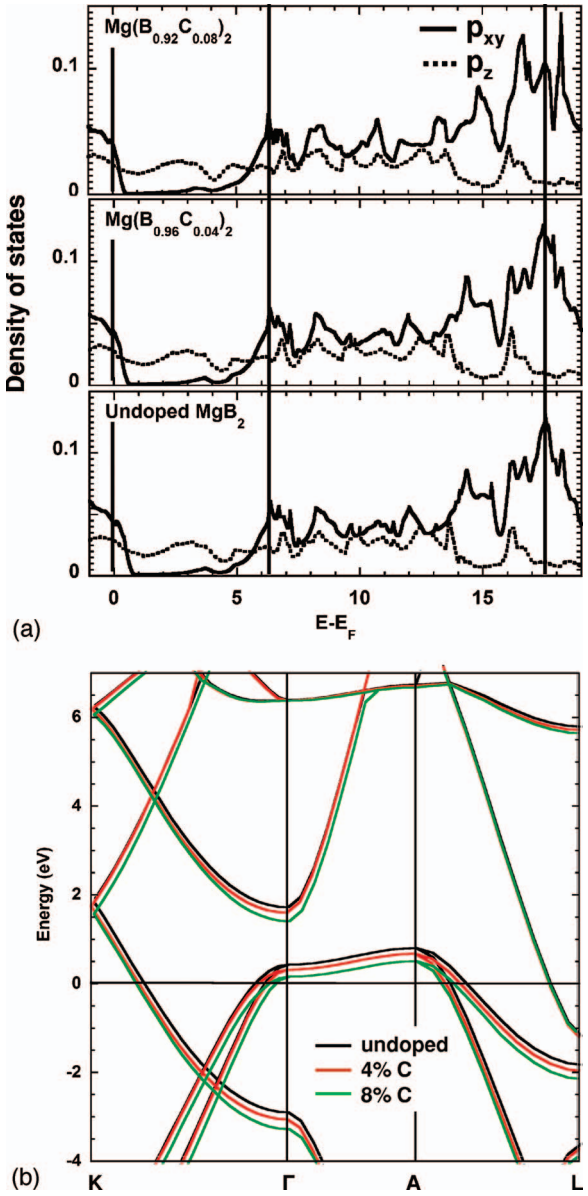

FIG. 9. (Color) Calculated (a) partial density of states and (b) band structure of pristine and C-doped MgB_2 showing the σ- and π-band shift for the different doping concentrations.

However, the large peak in the σ DOS at 17.5 eV shows several changes with increasing C concentration. The high intensity at 17.5 eV is decreasing in energy to 16.5 eV in $Mg(B_{0.92}C_{0.08})_2$, while the less intense peak at 18.2 eV in MgB_2 increases significantly in intensity to form the largest peak in the σ DOS in $Mg(B_{0.92}C_{0.08})_2$. These changes can explain the apparent shift of peak *c* in Fig. 4(a). The band structure for MgB_2, $Mg(B_{0.96}C_{0.04})_2$, and $Mg(B_{0.92}C_{0.08})_2$ [shown in Fig. 9(b)] further highlights the changes seen in the experiments and in the DOS. First, the flat σ band close to E_F is slowly shifting below the Fermi level with increasing C concentration, resulting in the σ band nearly reaching E_F at the Γ point for $Mg(B_{0.92}C_{0.08})_2$. However, the σ^* band does not seem to shift at all in energy for higher C doping. Interestingly, the π band can be seen to shift downward by 0.25 eV at *K* for $Mg(B_{0.92}C_{0.08})_2$. In contrast to the band-filling picture for Al doping, the shifts of both the σ and the π bands close to E_F in C-doped MgB_2 indicate that the additional electrons provided by the C atoms replacing B fill both the π and the σ states at the Fermi level. This filling of both bands in the case of C doping can explain why the relative pre-peak intensity of the B *K* edge overestimates the amount of C needed for T_c to reach 0 K.

CONCLUSIONS

In conclusion, we have shown that the combination of high-resolution *Z*-contrast imaging and EELS can be used to study the effects of electron doping on the σ and the π band of the two-band superconductor MgB_2. We have further shown that substituting either C for B, or Al for Mg, does not

results in any long-range ordered superstructures visible by TEM, in contrast to previously reports for high concentration of Al-doping concentrations.[42,43] Additionally, EELS revealed that the effect of electron doping on the electronic structure of MgB_2 is very similar for either dopant, while the superconducting transport properties of both samples are significantly different. We have presented both theoretical and experimental evidence that doping MgB_2 with electrons on the Mg and the B sites results in filling the σ hole-states close to the Fermi level and thus an increase in the Fermi level energy. This filling of the superconducting hole-state in the σ band with increasing doping concentration has been shown to be closely linked to the disappearance of the σ-band superconductivity once all these states are filled. Moreover, we have shown that the band filling for Al and C doping does not occur in a rigid band fashion; the σ^* bands in Al-doped MgB_2 shift faster than than σ bands close to E_F, while in C-doped MgB_2 the σ^* bands remain constant and the σ bands close the the Fermi level shift significantly.

In addition, our results clearly show that selective doping on either the Mg or the B site affects both bands of the B p states. More specifically, it was previously shown that there is a significant charge transfer of electrons from the B planes towards the Mg planes[44] and adding extra electrons on either lattice site should result in filling of both the σ and the π bands. Interestingly, we could show that only C doping results in a measurable filling of the π band, while Al doping does not influence the π-band DOS at all. Finally, we have presented experimental and theoretical evidence that the reduction of T_c for both Al- and C-doped MgB_2 can be explained in large part by the band-filling mechanism alone. Although an increase in interband scattering is not needed to explain the drop in T_c of our $Mg_{1-x}Al_x(B_{1-y}C_y)_2$ samples, we cannot affirmatively exclude effects such as increased interband scattering, local clustering of C atoms, or the buckling of C-doped boron planes to occur in $Mg(B_{1-y}C_y)_2$ and cause a further decrease T_c. However, in contrast to Al-doped MgB_2, the addition of C to MgB_2 has been shown to increase the upper critical field (H_{c_2}) significantly, which can be explained by the increase electron-hole scattering in the B planes and also results in a decrease in T_c. Our results presented in this paper suggest that adding additional holes on the Mg sites by doping for example with Na to offset the negative effects of C doping on the σ band, while keeping the C on the B site to increase H_{c_2} but without the loss of T_c, thus results in a new high-field, high-T_c superconductor

ACKNOWLEDGMENTS

This manuscript has been authored by Brookhaven Science Associates, LLC under Contract Nos. DE-AC02-98CH1-886 and DOE FG02 96ER45610 with the U.S. Department of Energy, Division of Materials Sciences, Office of Basic Energy Science. One author (RFK) acknowledges support as a Goldhaber Fellow at BNL. Other authors (LDC and AJZ) acknowledge additional support from the BNL-LDRD programs.

*E-mail address: klie@bnl.gov

[1] J. Nagamatsu, N. Nakagawa, T. Muranaka, Y. Zenitani, and J. Akimitsu, Nature (London) **410**, 63 (2001).
[2] A. Brinkman, A. A. Golubov, H. Rogalla, O. V. Dolgov, J. Kortus, Y. Kong, O. Jepsen, and O. K. Andersen, Phys. Rev. B **65**, 180517(R) (2002).
[3] A. Y. Liu, I. I. Mazin, and J. Kortus, Phys. Rev. Lett. **87**, 087005 (2001).
[4] S. Agrestini, D. Di Castro, M. Sansone, N. L. Saini, A. Saccone, S. De Negri, M. Giovannini, M. Colapietro, and A. Bianconi, J. Phys.: Condens. Matter **13**, 11689 (2001).
[5] K. Papagelis, J. Arvanitidis, K. Prassides, A. Schenck, T. Takenobu, and Y. Iwasa, Europhys. Lett. **61**, 254 (2003).
[6] H. Schmidt, J. F. Zasadzinski, K. E. Gray, and D. G. Hinks, Physica C **385**, 221 (2003).
[7] D. Di Castro, S. Agrestini, G. Campi, A. Cassetta, M. Colapietro, A. Congeduti, A. Continenza, S. De Negri, M. Giovannini, S. Massidda M. Nardone, A. Pifferi, P. Postorino, G. Profeta, A. Saccone, N. L. Saini, G. Satta, and A. Bianconi, Europhys. Lett. **58**, 278 (2002).
[8] P. Postorino, A. Congeduti, P. Dore, A. Nucara, A. Bianconi, D. Di Castro, S. De Negri, and A. Saccone, Phys. Rev. B **65**, 020507(R) (2001).
[9] A. Bianconi, S. Agrestini, D. Di Castro, G. Campi, G. Zangari, N. L. Saini, A. Saccone, S. De Negri, M. Giovannini, G. Profeta, Phys. Rev. B **65**, 174515 (2002).
[10] A. J. Zambano, A. R. Moodenbaugh, and L. D. Cooley, Supercond. Sci. Technol. **18**, 1411 (2005).
[11] G. Papavassiliou, M. Pissas, M. Karayanni, M. Fardis, S. Koutandos, and K. Prassides, Phys. Rev. B **66**, 140514(R) (2002).
[12] S. Margadonna, K. Prassides, I. Arvanitidis, M. Pissas, G. Papavassiliou, and A. N. Fitch, Phys. Rev. B **66**, 014518 (2002).
[13] M. Putti, M. Affronte, P. Manfrinetti, and A. Palenzona, Phys. Rev. B **68**, 094514 (2003).
[14] M. Putti, C. Ferdeghini, M. Monni, I. Pallecchi, C. Tarantini, P. Manfrinetti, A. Palenzona, D. Daghero, R. S. Gonnelli, and V. A. Stepanov, Phys. Rev. B **71**, 144505 (2005).
[15] J. Kortus, O. V. Dolgov, R. K. Kremer, and A. A. Golubov, Phys. Rev. Lett. **94**, 027002 (2005).
[16] H. D. Yang, H. L. Liu, J.-Y. Lin, M. X. Kuo, P. L. Ho, J. M. Chen, C. U. Jung, Min-Seok Park, and Sung-lk Lee, Phys. Rev. B **68**, 092505 (2003).
[17] R. S. Gonnelli, D. Daghero, A. Calzolari, G. A. Ummarino, V. Dellarocca, V. A. Stepanov, S. M. Kazakov, N. Zhigadlo, and J. Karpinski, Phys. Rev. B **71**, 060503(R) (2005).
[18] T. Masui, S. Lee, and S. Tajima, Phys. Rev. B **70**, 024504 (2004).
[19] T. Tomita, J. J. Hamlin, J. S. Schilling, D. G. Hinks, and J. D. Jorgensen, Phys. Rev. B **64**, 092505 (2001).
[20] A. V. Pogrebnyakov, X. X. Xi, J. M. Redwing, V. Vaithyanathan, D. G. Schlom, A. Soukiassian, S. B. Mi, C. L. Jia, J. E. Giencke, C. B. Eom J. Chen, Y. F. Hu, Y. Cui, and Q. Li,Appl. Phys. Lett. **85**, 2017 (2004).

[21] J. Karpinski, N. D. Zhugadlo, G. Schuck, S. M. Kazakov, B. Batlogg, K. Rogacki, R. Puzniak, J. Jun, E. Müller, P. Wägli *et al.*, Phys. Rev. B **71**, 174506 (2005).
[22] R. F. Klie, H. Su, Y. Zhu, J. W. Davenport, J. C. Idrobo, N. D. Browning, and P. D. Nellist, Phys. Rev. B **67**, 144508 (2003).
[23] R. F. Klie, J. C. Idrobo, N. D. Browning, A. Serquis, Y. T. Zhu, X. Z. Liao, and F. M. Muller, Appl. Phys. Lett. **80**, 3970 (2002).
[24] Y. Zhu, A. R. Moodenbaugh, G. Schneider, J. W. Davenport, T. Vogt, Q. Li, G. Gu, D. A. Fischer, and J. Tafto, Phys. Rev. Lett. **88**, 247002 (2002).
[25] L. D. Cooley, A. J. Zambano, A. R. Moodenbaugh, R. F. Klie, J.-C. Zheng, and Y. Zhu (unpublished).
[26] E. M. James and N. D. Browning, Ultramicroscopy **78**, 125 (1999).
[27] E. M. James, N. D. Browning, A. W. Nicholls, M. Kawasaki, Y. Xin, and S. Stemmer, J. Electron Microsc. **47**, 561 (1998).
[28] P. D. Nellist and S. J. Pennycook, Ultramicroscopy **78**, 111 (1999).
[29] R. F. Klie and Y. Zhu, Micron **36**, 219 (2005).
[30] J. M. Cowley, J. Electron Microsc. Tech. **3**, 25 (1986).
[31] R. F. Egerton, *Electron Energy Loss Spectroscopy in the Electron Microscope* (Plenum Press, New York, 1986).
[32] J. Fertig and H. Rose, Optik (Stuttgart) **59**, 407 (1981).
[33] N. D. Browning, J. Yuan, and L. M. Brown, Philos. Mag. A **67**, 261 (1993).
[34] P. Hohenberg and W. Kohn, Phys. Rev. **136**, B864 (1965).
[35] G. G. Parr and W. T. Yang, *Density-Functional Theory of Atoms and Molecules* (Oxford University Press, Oxford, 1989).
[36] P. Blaha, K. Schwarz, G. Madsen, D. Kvasnicka, and J. Luitz, *WIEN2k, An Augmented Plane* Wave+Local *Orbitals Program for Calculating Crystal Properties* (Techn. Universitat Wien, 2001).
[37] J. P. Perdew, K. Burke, and M. Ernzerhof, Phys. Rev. Lett. **77**, 3865 (1996).
[38] R. H. T. Wilke, S. L. Bud'ko, P. C. Canfield, D. K. Finnemore, R. J. Suplinskas, and S. T. Hannahs, Phys. Rev. Lett. **92**, 217003 (2004).
[39] R. F. Klie, Y. Zhu, G. Schneider, and J. Tafto, Appl. Phys. Lett. **82**, 4316 (2003).
[40] J. C. Idrobo, S. Ogut, T. Yildirim, R. F. Klie, and N. D. Browning, Phys. Rev. B **70**, 172503 (2004).
[41] R. Brydson, H. Sauer, W. Engel, J. M. Thomas, E. Zeitler, N. Kosugi, and H. Kuroda, J. Phys.: Condens. Matter **1**, 797 (1989).
[42] J. S. Slusky, N. Rogado, K. A. Regan, M. A. Hayward, P. Khalifah, T. He, K. Inumaru, S. M. Loureiro, M. K. Haas, H. W. Zandbergen and R. J. Cava, Nature (London) **410**, 343 (2001).
[43] H. W. Zandbergen, M. Y. Wu, H. Jiang, M. A. Hayward, M. K. Haas, and R. J. Cava, Physica C **366**, 221 (2002).
[44] L. J. Wu, Y. M. Zhu, T. Vogt, H. B. Su, J. W. Davenport, and J. Tafto, Phys. Rev. B **69**, 064501 (2004).